Direct observation of dynamics of thermal expansion using pump-probe high-energy-resolution x-ray diffraction

S. Stoupin,* A. M. March, H. Wen, D. A. Walko, Y. Li, E. M. Dufresne, S. A. Stepanov, K.-J. Kim, and Yu. V. Shvyd'ko†
Advanced Photon Source, Argonne National Laboratory, Argonne, Illinois 60439, USA

V. D. Blank and S. A. Terentyev
Technological Institute for Superhard and Novel Carbon Materials, Troitsk, Russia

(Received 10 April 2012; revised manuscript received 11 June 2012; published 2 August 2012)

Time evolution of thermal expansion in the crystal lattice of diamond was studied on the time scale from 100 ps to 18 μs upon heating of the crystal through the entire thickness by a penetrating optical laser pulse of $\approx$8 ps in duration. Bragg reflectivity curves were measured at different instants of time using pump-probe high-energy-resolution x-ray diffraction with $\simeq 10^{-8}$ strain sensitivity. The observed time-dependent variation of Bragg reflectivity was found to be in agreement with dynamical diffraction calculations for a crystal with propagating strain generated by thermally induced stress. The strain propagated at the speed of sound for longitudinal waves from both crystal surfaces into the bulk.

DOI: 10.1103/PhysRevB.86.054301 PACS number(s): 65.40.De, 61.05.cp, 62.30.+d

I. INTRODUCTION

How fast does a body expand if heated instantaneously? In most experimental situations the prevailing factor in the time evolution of thermal expansion is the process of reaching thermal equilibrium via various mechanisms of heat transfer (heat conduction, mass transfer, thermal radiation). Only a few studies consider full-scale dynamics of thermal expansion apart from heat transfer.[1–3] Meanwhile, it is understood that in the absence of heat transfer, mechanical disturbances caused by the induced thermal stress propagate with the speed of sound. Transient lattice dynamics has been extensively studied using the optical pump–x-ray probe method for opaque solids with submicron penetration depths ($\zeta \lesssim 1$ μm) for the optical pump radiation.[4–9]

For example, Kojima *et al.*[4] studied lattice dynamics of silicon and found that the lattice expansion in the lateral direction due to pulsed-laser irradiation was negligible. Chin *et al.*[6] and Rose-Petruck *et al.*[5] presented a rather clear picture for dynamics of thermal expansion in the initial regime upon generation of thermal stress due to the absorbed laser pulse. Lattice strain initiates at the surface (due to absence of confinement in the direction normal to the surface) and propagates into the bulk with the speed of sound for longitudinal waves. Mechanical relaxation of the impulsively stressed submicron lattice layer occurs as the strain propagates through that layer (i.e., subnanosecond time interval). It was found that in this time regime the lattice dynamics is well described by the thermoelastic model of Thomsen *et al.*[10] However, strong temperature gradients yield substantial heat diffusion with characteristic times ζ^2/κ (κ is the thermal diffusivity) on the nanosecond time scale and temperature variation in the material properties. Therefore, it is unclear if diffusive heat transfer plays a significant role in dynamics of thermal expansion, especially beyond the submicron penetration depths. Furthermore, due to high energy density deposited in the submicron surface layer, other mechanisms of heat and energy transfer may play a significant role in strain propagation. For example, if dense electron-hole plasma is generated at the crystal surface, the strain front may propagate into the bulk faster than the speed of sound.[8]

Along with pure fundamental interest, there are practical needs for detailed understanding of the dynamics of thermal expansion and the underlying physics. Knowledge of the dynamics of thermal expansion of flash-heated solids is important in studies involving ultrashort (fs to ps duration) pulses of penetrating hard x-rays generated by x-ray free-electron lasers (XFELs). In particular, recent advances in the development of fully coherent hard x-ray sources, self-seeded XFELs[11–13] and XFEL oscillators (XFELO),[14–17] rely on extensive use of x-ray crystal optics under heat load of the ultrashort x-ray pulses. Knowledge of the dynamics of thermal expansion is vital for proper performance of the x-ray optics in these projects.

In this work we study a time response of the C (diamond) crystal lattice to a thermal stress induced across the entire sample thickness by a penetrating optical laser pulse. In order to rapidly deposit heat through the entire crystal thickness, pulsed laser excitation was chosen at a wavelength of 400 nm, which is substantially below the optical absorption edge of diamond at 225 nm. A special diamond crystal of thickness $d \simeq 200$ μm with enhanced absorption at 400 nm (absorption length $\zeta \simeq 380$ μm) was utilized. To minimize the influence of nonlinear effects induced by the laser radiation, such as radiation damage, generation of shock waves, and nonlinear optical absorption, low-flux laser pulses ($\approx$9 GW/cm^2) of $\approx$8 ps in duration were utilized. Thus, upon the interaction with the laser pulse, temperature gradient and heat transfer across the sample thickness were minimized. The lattice response was directly probed using high-energy-resolution x-ray diffraction. Hard x-ray synchrotron radiation (x-ray energy $E_X \simeq 13.9$ keV) with an energy bandwidth $\Delta E_X \approx 1.5$ meV was utilized to measure Bragg reflectivity curves of the C 008 reflection in backscattering at different instants of time. The expected increase in the crystal temperature is only a fraction of Kelvin per pulse. Under these conditions, the use of a high-energy-resolution x-ray diffraction technique with $\approx 10^{-8}$ strain resolution[18,19] was crucial.

Three time regimes were studied. In the initial regime, 0–10 ns, it was found that an onset value corresponding to the initial averaged level of thermal expansion occurs due to strain propagating into the depth of the crystal with the speed of sound for longitudinal waves. Time-dependent asymmetric distortion of the reflectivity curves was observed in agreement with dynamical diffraction simulations using the expected propagating strain profiles. In the second regime, 10 ns $<$ 1 μs, a strain standing wave across the thickness of the crystal is established and the lattice parameter oscillates about the onset value. In the third regime ($>$1 μs), equilibration of the lattice parameter is observed due to heat dissipation.

II. THEORY

To describe strain profiles in diamond crystal induced by an absorbed optical laser pulse we employ the thermoelastic model developed by Thomsen *et al.*[10] However, our solution has a different form since the absorption length for the laser radiation ζ is comparable with the diamond thickness d. If Q_a is the absorbed energy of the laser pulse, and A is the area over which the energy is absorbed ($\sqrt{A} \gg d$), the temperature profile at the sample depth z is given by

$$\Delta T(z) = \Delta T_0 e^{-\frac{z}{\zeta}}, \quad \Delta T_0 = \frac{\gamma Q_a}{A\rho c\zeta(1-e^{-\frac{d}{\zeta}})}, \tag{1}$$

where ρ is the density, c is the specific heat capacity for diamond, and γ is the fraction of the absorbed energy Q_a transferred to the lattice. Here, we do not calculate γ explicitly but keep it as a free parameter. The laser pulse below the diamond optical absorption edge generates carriers due to ionization of defect states in diamond. It is expected that these carriers will relax by emitting phonons within a few picoseconds. Since our approach is limited to a time resolution of $\approx$100 ps, we assume that the energy is transferred to the lattice instantaneously.

For simplicity, we neglect the intrinsic anisotropy and the Poisson effect (the Poisson's ratio of diamond is only $\nu \simeq 0.07$) and assume that the strain $\eta(z,t) = \partial u(z,t)/\partial z$ is only along the z direction. The equations of elasticity to be solved are

$$\sigma_{zz} = Y\frac{\partial u(z,t)}{\partial z} - \alpha Y \Delta T(z), \tag{2}$$

$$\rho\frac{\partial^2 u(z,t)}{\partial t^2} = \frac{\partial \sigma_{zz}}{\partial z}, \tag{3}$$

where Y is the Young's modulus, α is the linear thermal expansion coefficient, and ρ is the mass density. The boundary conditions are that the stress [Eq. (2)] vanishes at the crystal boundaries $z = 0$ and $z = d$. At $t = 0$, $\partial u/\partial z = 0$ and $\partial u/\partial t = 0$. The solution is given by

$$\eta(z,t) = \alpha\big(\Delta T(z) - \tfrac{1}{2}[F(n,z-vt) + F(n,z+vt)]\big). \tag{4}$$

Here, $v = \sqrt{Y/\rho}$ is the speed of sound for longitudinal waves. The function $F(n,x)$ is defined on intervals $[nd < x < (n+1)d]$ $(n = 0,1,2,\ldots)$. The initial and boundary conditions yield the following iterative procedure to calculate the solution:

$$\begin{aligned} &F(0,x) = \Delta T(x), \quad F(-n,x) = -F(n-1,-x), \\ &F(n,x) = -F(-n+1,2d-x). \end{aligned} \tag{5}$$

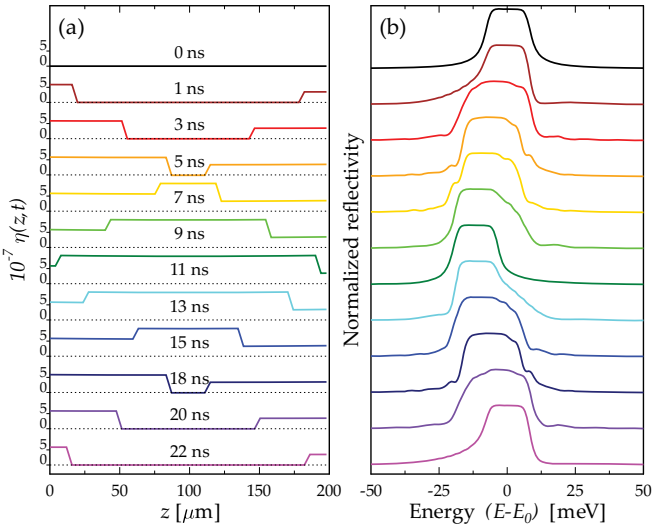

FIG. 1. (Color online) (a) Thermally induced strain profiles in diamond of thickness $d = 200$ μm at various times after the arrival of the optical laser pulse. (b) Theoretical Bragg backscattering reflectivity curves of the C 008 reflection obtained numerically using dynamical theory of x-ray diffraction[20] with the corresponding strain profiles.

Thus, strain profiles can be obtained at any point of time using Eqs. (4) and (5). The interaction time of the x rays with diamond is about the length of a synchrotron x-ray pulse ($\lesssim$100 ps). Therefore, x-ray diffraction probes a snapshot of the crystal lattice profile at a certain time as strain propagates in the z direction. The strain profiles derived above were utilized in dynamical diffraction calculations to obtain reflectivity curves of the strained diamond at different times. The calculations were based on the recursion matrix method.[20]

The strain profiles are shown in Fig. 1(a) for different times upon absorption of a penetrating laser pulse resulting in the temperature profile of Eq. (1) ($\gamma = 1$). The corresponding simulated reflectivity curves in backscattering are shown in Fig. 1(b). These curves were convoluted with a Gaussian curve of 3 meV width to simulate the effect of an instrument resolution function. We note that if at any given time the strain distribution is nonuniform, the shape of the reflectivity curve is distorted compared to the shape of the original unperturbed curve at $t = 0$. At times $t_n = nd/v$ the strain wave fronts originated at the surfaces $z = 0$ and $z = d$ propagate through the entire thickness of the crystal, yielding a nearly uniform distribution of strain at an increased level. The shape of the resulting reflectivity curve is close to that of the unperturbed one and the curve is shifted from the original position $E = E_0$ by $\Delta E \approx 2\alpha\Delta T_0 E_X$. Thus, time-resolved measurements of x-ray diffraction intensity at a fixed energy on either slope of the reflectivity curve would yield distorted oscillations due to the evolving strain profiles.

III. EXPERIMENTAL

The experimental setup for pump-probe high-energy-resolution x-ray diffraction is shown in Fig. 2. A four-bounce high-resolution monochromator (HRM) was used to

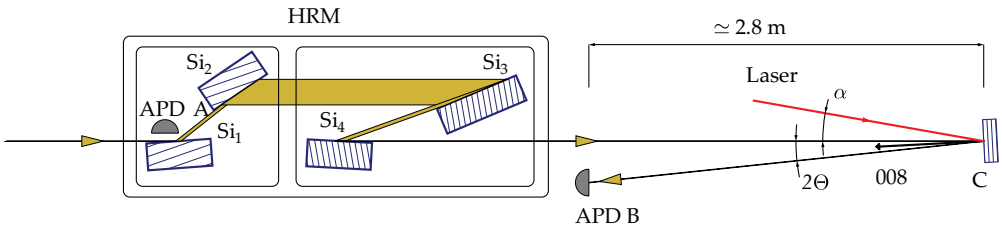

FIG. 2. (Color online) Experimental setup (see text for details).

produce x rays with an energy bandwidth $\Delta E_X \approx 1.5$ meV.[21] An avalanche photodiode (APD A) measuring radiation scattered from the first crystal (Si_1) of the HRM was used for normalization purposes. To measure the backscattered signal, another avalanche photodiode (APD B) was placed after the HRM at a small angular offset $2\Theta \approx 2.5 \times 10^{-3}$ from the monochromatic beam incident to the diamond crystal. The angle of incidence for the laser beam was $\alpha \approx 15$ deg. The second harmonic of a Ti:sapphire laser (primary wavelength 800 nm) was used. In order to enhance absorption of the 400-nm laser radiation, a nitrogen-doped diamond (type Ib) of high crystalline quality was utilized. The crystal was grown at the Technological Institute for Superhard and Novel Carbon Materials (Troitsk, Russia) using the temperature-gradient method at high static pressure and temperature in a Fe-Co-C system. Nitrogen concentration measured by Fourier transform infrared spectroscopy (FTIR) was about 80 ppm. After the crystallization process, the diamond crystal was cut using a laser and mechanically polished to fabricate a plate with $3.0 \times 3.0 \times 0.2$ mm^3 dimensions. The synchrotron x-ray pulse train (6.5-MHz repetition rate) and the laser pulse train (1-kHz repetition rate) were synchronized, and the delay between the two was electronically controlled.[22] Time gates were formed by a multichannel delay generator and assigned to the x-ray pulses as follows. The first gate selected an x-ray pulse that was incident on the diamond before the arrival of the laser pulse (*laser off* signal). The second gate was set on the x-ray pulse that arrives to the sample at a time delay $\Delta\tau$ after the laser pulse (*laser on* signal). Several additional gates were assigned to consecutive synchrotron x-ray pulses separated by $\Delta\tau_p \simeq 153$ ns. Thus, the signals in the gated channels represented x-ray intensity reflected at times $\tau = \Delta\tau + (m - 2)\Delta\tau_p$, where m is the gate number. In this data-collection scheme, an energy scan of the HRM yields reflectivity curves at times τ. Prior to data collection, temporal and spatial overlap was achieved between the x-ray beam (size $\simeq 100$ μm) and the laser beam (size $\simeq 350$ μm) on the sample surface.

IV. RESULTS AND DISCUSSION

In the first step, Bragg reflectivity curves were measured at different time intervals upon the arrival of the laser pulse. Figure 3 shows selected reflectivity curves that correspond to a *total* (static) curve, a time-resolved curve before the arrival of the laser pulse (*laser off*), and a time-resolved curve at $\tau = 4$ ns after the arrival of the laser pulse (*laser on*). The experimentally observed single-peak curve with FWHM $\simeq$ 26.7 meV confirms high crystal quality for type Ib crystal. The *laser off* curve matches the *total* curve, indicating that the crystal lattice is in a stationary state most of the time between the laser pulses. In contrast, the *laser on* curve is shifted to lower energies. The low-energy slope of the curve is shifted further than the high-energy slope. Such asymmetric distortion is expected (see Fig. 1).

In the next step, the ratio of the normalized *laser on (off)* backscattering intensities, $\Gamma_\pm = I_\pm^{\rm on}/I_\pm^{\rm off}$, was measured at fixed energy positions $E_\pm$ on the slopes of the curve as a function of time. To maximize the sensitivity of the measurement method these energy positions were chosen at the inflection points. Since the energy shifts for each slope are small, they can be expressed through the values of derivative $R'(E) = dR(E)/dE$ of the *total* reflectivity curve $R(E)$. The intensity variation was converted to a variation of the lattice parameter $\Delta a/a$ (i.e., strain) as follows:

$$\left(\frac{\Delta a}{a}\right)_\pm = \frac{\Gamma_\pm - 1}{E_X R'(E_\pm)/R(E_\pm)}. \qquad (6)$$

In the first experiment data were subsequently collected for each slope in the time interval from 0 to 9 ns with an increment of either 50 or 100 ps. In the second experiment data were collected for each energy slope up to about 760 ns with an increment of 1 ns. In the third experiment data were collected on the low-energy slope in multiple steps covering a region up to 18.2 μs. The resulting strain variation is shown in Fig. 4 in three time regimes. Figure 4(a) shows the dynamics of thermal

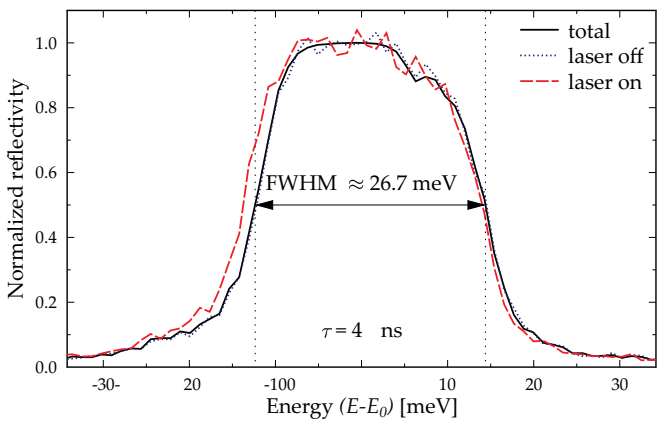

FIG. 3. (Color online) The effect of the absorbed laser pulse on the Bragg reflectivity curve of the diamond crystal: a *total* (static) reflectivity curve (solid line), a time-resolved curve before the laser pulse arrival (dotted line), and a time-resolved curve at 4 ns after the laser pulse arrival (dashed line).

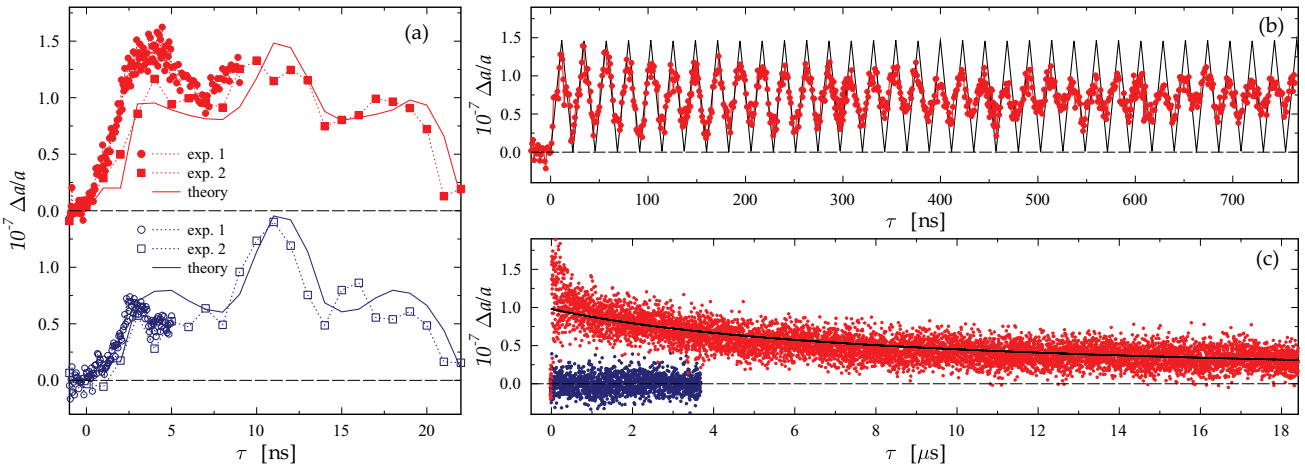

FIG. 4. (Color online) Dynamics of thermal expansion in diamond measured at the slopes of the Bragg reflectivity curve. (a) Thermal expansion measured at the low-energy slope (top, red) and the high-energy slope (blue, bottom) of the reflectivity curve in the time interval of the first period of strain oscillations. The experimental data (experiments 1 and 2) are shown by markers. The solid lines are the results of dynamical diffraction simulations with strain profiles [Eq. (4)]. (b) Strain oscillations due to the strain standing wave. The results of experiment 2 averaged for the low-energy and high-energy slopes are shown by red circles and lines. The sawtooth-like curve (black line) represents the strain profiles [Eq. (4)] averaged across the thickness of the diamond crystal. (c) The strain oscillates about a decaying baseline on the μs time scale. Experimental data (experiment 3, red circles) were collected on the low-energy slope. The decaying baseline (black) is an approximation for thermal strain relaxation due to heat conduction in the radial direction (numerical simulation). The blue circles represent the *laser off* signal fluctuating about zero and thus reflect the noise level [$\approx 10^{-8}$ (rms)].

expansion on a time interval corresponding to the first period of strain oscillations. The shapes of experimental curves are in agreement with those of the theoretical curves obtained using Eq. (4) combined with the dynamical diffraction simulations. The theoretical curves were scaled using $\gamma = 0.15$. Comparing the rise time of the experimental and the theoretical curves, we conclude that the onset of thermal expansion occurs with the speed of longitudinal strain waves propagating from both crystal surfaces into the bulk. The onset is established at an observation time of $\simeq$5 ns when the strain wave fronts propagated halfway through the thickness of the crystal. Figure 4(b) shows strain oscillations due to the longitudinal standing wave formed in the crystal. Data of experiment 2 are shown by red circles and line. The sawtooth-like black solid line is the strain [Eq. (4)] averaged across the thickness of the crystal (an approximation that corresponds to incoherent superposition of x rays reflected from all the atomic layers). The speed of sound for longitudinal waves calculated from the measured period of the oscillations is $v \simeq 17.4$ km/s. We note that the amplitude of the strain oscillations decays. This can be due to strain propagation in the lateral direction as well as due to sound dissipation, phenomena that are not taken into account in our theoretical model. Data collected in experiment 3 are shown in Fig. 4(c). Here, the strain continues to oscillate about a decaying baseline $\eta_0(\tau) \simeq \alpha \Delta T_0(\tau)$. The curve that approximates this decaying baseline is the result of numerical simulation for $\Delta T_0(\tau)$ temperature relaxation due to one-dimensional (radial direction) heat conduction in diamond. Here, the characteristic time for relaxation of the lattice parameter is $\approx$10 μs. The data fluctuating about zero corresponds to the *laser off* signal and thus reflects a noise level of $\approx 10^{-8}$ (rms). We note that the strain oscillations were clearly resolved only at $\tau \lesssim 1$ μs.

V. CONCLUSIONS

In conclusion, we measured dynamics of thermal expansion in a single-crystal diamond upon heating by a low-flux optical laser pulse through the entire sample thickness (200 μm). Thus, temperature gradient and heat transfer across the sample thickness were minimized. The measurements were performed using high-energy-resolution x-ray diffraction (diamond 008 reflection in backscattering) with strain sensitivity of $\approx 10^{-8}$. We have shown that in the initial regime of a few nanoseconds, the development of the onset of thermal expansion is solely due to thermally induced strain propagating with the speed of sound for longitudinal waves from both crystal surfaces into the bulk. Time-dependent asymmetric distortion of the reflectivity curves was observed in agreement with dynamical diffraction simulations using the expected propagating strain profiles. In the second time regime, a strain standing wave across the thickness of the crystal is established, and the lattice parameter oscillates about the onset value. The amplitude of these oscillations decays with a relaxation time on the order of 1 μs. In the third time regime, the onset value decays as a result of heat conduction away from the probed region. Thus, in absence of heat transfer, the dynamics of thermal expansion is due to strain propagation with the speed of sound and the relevant time scales can extend far beyond observation times of $\approx$1 ns.

The results of this study provide practical guidance on dynamics of thermal expansion of a realistic optical element under the heat load of a pulse train of penetrating radiation with a pulse duration of a few picoseconds. The dynamics of thermal expansion alone should not deteriorate Bragg reflectivity of the optical element during the interaction time of the lattice with the radiation pulse. The results are of major importance for the development of x-ray optics for the XFELO and high-repetition-rate XFEL.

ACKNOWLEDGMENTS

We thank H. Sinn for his input on heat-transfer calculations in diamond and A. Kirichenko for measuring optical absorption of the diamond sample. The help of our colleagues T. Roberts, K. Goetze, D. Shu, B. Adams, H. Gibson, and A. Deriy is greatly appreciated. Use of the Advanced Photon Source was supported by the US Department of Energy, Office of Science, Office of Basic Energy Sciences, under Contract No. DE-AC02-06CH11357.

---

*sstoupin@aps.anl.gov
†shvydko@aps.anl.gov

[1] D. W. Tang, B. L. Zhou, H. Cao, and G. H. He, Appl. Phys. Lett. **59**, 3113 (1991).
[2] Y. C. Lee, J. Phys.: Condens. Matter **20**, 055202 (2008).
[3] Y. C. Lee, J. Phys.: Condens. Matter **21**, 325702 (2009).
[4] S. Kojima, K.-Y. Liu, Y. Kudo, S. Kawado, T. Ishikawa, and T. Matsushita, Jpn. J. Appl. Phys. **33**, 5612 (1994).
[5] C. Rose-Petruck, R. Jimenez, T. Guo, A. Cavalleri, C. W. Siders, F. Rksi, J. A. Squier, B. C. Walker, K. R. Wilson, and C. P. J. Barty, Nature (London) **398**, 310 (1999).
[6] A. H. Chin, R. W. Schoenlein, T. E. Glover, P. Balling, W. P. Leemans, and C. V. Shank, Phys. Rev. Lett. **83**, 336 (1999).
[7] D. A. Reis, M. F. DeCamp, P. H. Bucksbaum, R. Clarke, E. Dufresne, M. Hertlein, R. Merlin, R. Falcone, H. Kapteyn, M. M. Murnane, J. Larsson, Th. Missalla, and J. S. Wark, Phys. Rev. Lett. **86**, 3072 (2001).
[8] M. F. DeCamp, D. A. Reis, A. Cavalieri, P. H. Bucksbaum, R. Clarke, R. Merlin, E. M. Dufresne, D. A. Arms, A. M. Lindenberg, A. G. MacPhee, Z. Chang, B. Lings, J. S. Wark, and S. Fahy, Phys. Rev. Lett. **91**, 165502 (2003).
[9] K. Sokolowski-Tinten and D. von der Linde, J. Phys.: Condens. Matter **16**, R1517 (2004).
[10] C. Thomsen, H. T. Grahn, H. J. Maris, and J. Tauc, Phys. Rev. B **34**, 4129 (1986).
[11] G. Geloni, V. Kocharyan, and E. Saldin, J. Mod. Opt. **58**, 1391 (2011).
[12] R. R. Lindberg and Y. V. Shvyd'ko, Phys. Rev. Spec. Top.–Accel. Beams **15**, 050706 (2012).
[13] J. Amann, W. Berg, V. Blank, F.-J. Decker, Y. Ding, P. Emma, Y. Feng, J. Frisch, D. Fritz, J. Hastings, Z. Huang, J. Krzywinski, R. Lindberg, H. Loos, A. Lutman, H.-D. Nuhn, D. Ratner, J. Rzepiela, D. Shu, Yu. Shvyd'ko, S. Spampinati, S. Stoupin, S. Terentiev, E. Trakhtenberg, D. Walz, J. Welch, J. Wu, A. Zholents, and D. Zhu, Nature Photonics (in press).
[14] K.-J. Kim, Y. Shvyd'ko, and S. Reiche, Phys. Rev. Lett. **100**, 244802 (2008).
[15] K.-J. Kim and Y. V. Shvyd'ko, Phys. Rev. Spec. Top.–Accel. Beams **12**, 030703 (2009).
[16] Y. V. Shvyd'ko, S. Stoupin, A. Cunsolo, A. Said, and X. Huang, Nat. Phys. **6**, 196 (2010).
[17] Y. V. Shvyd'ko, S. Stoupin, V. Blank, and S. Terentyev, Nat. Photon. **5**, 539 (2011).
[18] S. Stoupin and Y. V. Shvyd'ko, Phys. Rev. Lett. **104**, 085901 (2010).
[19] S. Stoupin and Y. V. Shvyd'ko, Phys. Rev. B **83**, 104102 (2011).
[20] S. A. Stepanov, E. A. Kondrashkina, R. Köhler, D. V. Novikov, G. Materlik, and S. M. Durbin, Phys. Rev. B **57**, 4829 (1998) (online simulator available at http://x-server.gmca.aps.anl.gov/).
[21] S. Stoupin, Y. Shvyd'ko, D. Shu, R. Khachatryan, X. Xiao, F. DeCarlo, K. Goetze, T. Roberts, C. Roehrig, and A. Deriy, Rev. Sci. Instrum. **83**, 023105 (2012).
[22] E. M. Dufresne, B. Adams, D. A. Arms, M. Chollet, E. C. Landahl, Y. Li, D. A. Walko, and J. Wang, AIP Conf. Proc. **1234**, 181 (2010).